Hindawi
Geofluids
Volume 2019, Article ID 5874849, 9 pages
https://doi.org/10.1155/2019/5874849

Research Article

Experimental Investigation on Nonlinear Flow Anisotropy Behavior in Fracture Media

Chun Zhu,[1,2,3] **Xiaoding Xu**,[1,2] **Xiuting Wang**,[3,4] **Feng Xiong**,[3,5] **Zhigang Tao**,[2] **Yun Lin**,[3,6] **and Jing Chen**[2]

[1]*College of Construction Engineering, Jilin University, Changchun 130026, China*
[2]*State Key Laboratory for Geomechanics & Deep Underground Engineering Beijing, China University of Mining & Technology, Beijing 100083, China*
[3]*School of Civil, Environmental and Mining Engineering, The University of Adelaide, Adelaide, SA 5005, Australia*
[4]*School of Civil Engineering and Architecture, Anhui University of Science and Technology, Huainan 232000, China*
[5]*School of Civil Engineering, Wuhan University, Hubei 430072, China*
[6]*School of Resource and Safety Engineering, Central South University, Changsha, Hunan 410083, China*

Correspondence should be addressed to Feng Xiong; whufengx@163.com and Zhigang Tao; zhigangtao_cumtb@126.com

Received 26 February 2019; Accepted 9 June 2019; Published 24 June 2019

Guest Editor: Frédéric Nguyen

A series of flow experiments were performed on matched fractures to study the problem of non-Darcy flow in fractured media. Five rock fractures of different roughness were generated using indirect tensile tests, and their surface topographies were measured using a stereo topometric scanning system. The fracture was assumed to be a self-affine surface, and its roughness and anisotropy were quantified by the fractal dimension. According to the flow tortuosity effect, the nonlinear flow was characterized by hydraulic tortuosity and surface tortuosity power law relationships based on Forchheimer's law. Fracture seepage experiments conducted with two injection directions (0° and 90°) showed that Forchheimer's law described the nonlinear flow well. Both the proposed model and Chen's double-parameter model gave similar results to the experiment, but the match was closer with the proposed model. On this basis, a new formula for the critical Reynolds number is proposed, which serves to distinguish linear flow and Forchheimer flow.

1. Introduction

A long history of geological and human activities has caused most rock masses to be cut by a large number of faults and fractures [1–5]. These discontinuities form the main channels for groundwater flow, which control the permeability characteristics of the rock mass. In the study of rock mass hydrology, discontinuities are usually generalized into two smooth parallel plates, and the famous cubic law is hence obtained through theory and experiment. A variety of correction models [6–11] has been proposed to account for fracture roughness, contact, or filling.

Some engineering projects involve a high hydraulic gradient, for example, dam construction in the deep weak overburden of a river valley, exploitation of low-permeability oil and gas wells, and coal mine gas outbursts [12–16]. Under this condition, fluid flow through fractures is not linear, and the use of the cubic law or related modified models would cause large deviations. The well-known Forchheimer law is used to describe this flow behavior:

$$\nabla P = AQ + BQ^2, \tag{1}$$

where ∇P is the pressure gradient between the inlet and outlet of the fracture, Q is the flow rate through the fracture, and A and B are the coefficients of viscosity and inertia, respectively. Zimmerman et al. [17] observed the Forchheimer flow phenomena of rough fractures when the Reynolds number $\mathrm{Re} > 20$ through experiments and numerical methods. Zhang and Nemcik [18] discussed the linear and nonlinear flow

characteristics of rough fractures under different confining pressures. Zhou et al. [19] explained the physical significance of the Forchheimer flow coefficients A and B and the internal transition mechanism on the basis of water pressure tests under different confining pressures. However, the effects of fracture roughness on flow were not explained in detail. Jin et al. (2013) pointed out that the influence of a rough geometry on fracture flow is manifested in three aspects: the frictional effect in the fluid, the tortuous effect of the fracture surface, and a local roughness effect. Tsang [20] considered that the roughness of the fracture surface would lead to flow tortuosity, and Xiao et al. [21] introduced a tortuosity factor to describe the tortuosity of flow. Watanabe et al. [22] carried out fluid flow experiments in fractures with shear displacements and found that the nonlinear flow effect decreases as shear increases.

Fractal geometry was first put forward by B.B. Mandelbrot. Xie and Wang [23] introduced it into the description of fracture roughness and then used it to describe fluid flow characteristics at rock fracture surfaces. Murata and Saito [24] studied the influence of fractal parameters on the tortuosity effect, and Wang et al. [25] put forward a flow model using fractal parameters. Ju et al. [26] carried out flow experiments on rough single fractures with different fractal dimensions. These flow tests clarified the influence of a rough structure on seepage flow. Develi and Babadagli [27] carried out saturated seepage tests on seven kinds of artificial tensional fracture surfaces, describing the roughness of the fractures by means of the fractal dimension and discussing the influences of roughness, anisotropy, and normal stress on seepage characteristics.

In this paper, a nonlinear fractal model for rough fractures is deduced based on the tortuous effect and the self-affine fractal characteristics of the fracture surface. The law and anisotropy of Forchheimer flow are analyzed, and the new model is verified by seepage tests.

2. Nonlinear Fractal Model for Rough-Walled Rock Fractures

Forchheimer's law is composed of a linear part AQ and a nonlinear part BQ^2. When the flow rate is low, a cubic law can be used to describe the relationship of the flow rate and pressure. Hence, A can be expressed as

$$A = \frac{12\mu}{we_h^3}, \tag{2}$$

where μ is the dynamic coefficient of viscosity of the fluid and w is the width of the fracture. e_h is the hydraulic aperture, which can be calculated as $e_h = (12\mu Q/w/\nabla P)^{1/3}$.

The coefficient B represents the degree that the seepage curve deviates from that in the linear stage. Schrauf and Evans [28] put forward a form of B using dimensional analysis:

$$B = b_D \frac{\rho}{e_h^3 w^2}, \tag{3}$$

where ρ is the fluid density and b_D is a parameter related to the roughness of the fracture surface. Chen et al. [6] used the peak asperity height to describe fracture roughness and obtained a two-parameter model for b_D:

$$b_D = a\left(\frac{\xi}{2e_h}\right)^b, \tag{4}$$

where a and b are fitting parameters, respectively. However, the peak asperity height does not account for flow tortuosity and anisotropy. Chen et al. [6] also used numerical simulation to study non-Darcy behavior in fracture flow. The results showed that the rougher the surface was, the more tortuous the flow would be, and eddy currents and recirculation would occur at high velocity, which would increase the inertial resistance. In order to characterize the effect of flow tortuosity, the following power law relations are proposed by Murata and Saito [24] and Ji et al. (2015):

$$b_D = c\tau^a \tau_s^b, \tag{5}$$

where a, b, and c are fitting parameters. τ is the hydrological curvature, which is defined as the ratio of the actual length L_t of the seepage path to the horizontal length L_c along the pressure gradient of the fracture. τ_s is the curvature of the surface, which is defined as the ratio of the surface area to the projection area of the fracture surface.

For fractal fractures, the relationship between measure $F(\delta)$ and measurement scale δ is as follows:

$$F(\delta) = F_0 \delta^\alpha, \tag{6}$$

where α is a parameter related to the fractal dimension D and D is in the range 1-3. F_0 is the apparent measurement. Based on this, the relationship between the fracture surface area A_s and a square mesh with dimension δ_1 is as follows:

$$A_s = F_1 \delta_1^{2-D_s}, \tag{7}$$

where D_s is the fractal dimension of the fracture area. For a square fracture, when δ_1 is equal to L_c and equation (7) is substituted into $A_s(L_c) = A_c$, F_1 can be obtained as follows:

$$F_1 = A_c^{D_s/2}. \tag{8}$$

Hence, τ_s can be obtained:

$$\tau_s = \frac{A_s(\delta_1)}{A_c} = \left(\sqrt{\left(\frac{\delta_1^2}{A_c}\right)}\right)^{2-D_s}. \tag{9}$$

In addition, the fractal relationship of the length of the seepage path L_t and measure δ_2 is as follows:

$$L_t(\delta_2) = F_2 \delta_2^{1-D_T}, \tag{10}$$

where D_T is the fractal dimension of the seepage path. When δ_2 is equal to L_c and equation (10) is substituted into $L_t(L_c) = L_c$, F_2 can be obtained as

$$F_2 = L_c^{D_T}. \tag{11}$$

Hence, τ can be obtained:

$$\tau = \frac{L_t(\delta_2)}{L_c} = \left(\frac{\delta_2}{L_c}\right)^{1-D_T}. \tag{12}$$

Mandelbrot, the founder of fractal theory, suggested that the fractal dimension of the surface could be calculated by adding the dimension of a surface profile to 1. Therefore, the relationship between the fractal dimension of the profile length and the fractal dimension of the area is as follows:

$$D_s = D_l + 1. \tag{13}$$

Jin et al. [29] considered D_l as equal to D_T. Hence, b_D can be obtained by substituting equation (9) and equation (12) into equation (5):

$$b_D = c\left(\frac{\delta_2}{L_c}\right)^{a(1-D_l)}\left(\sqrt{\frac{\delta_1^2}{A_c}}\right)^{b(1-D_l)}. \tag{14}$$

When δ_1 and δ_2 are e_h, equation (1) becomes

$$b_D = c\left(\frac{e_h}{L_c}\right)^{(a+b)(1-D_l)}. \tag{15}$$

Hence, a new model of parameter B in Forchheimer's law can be obtained:

$$B = a\left(\frac{e_h}{L_c}\right)^{b(1-D_l)}\frac{\rho}{e_h^3 w^2}, \tag{16}$$

where a and b are constants that can be determined with fracture permeability tests. Firstly, the fractal dimension is calculated from fracture surface data. The curve relating flow to pressure gradient is then obtained through fracture permeability tests, and this is used to obtain a and b.

3. Fracture Surface Measurement

3.1. Rock Fracture Preparation. The effect of fracture surface roughness on fluid flow was studied by way of saturated seepage tests of rock fracture surfaces of different roughness. A natural fracture surface is difficult to obtain, so artificial tension fracture specimens were used to study the characteristics of fluid flow in fractures. In this study, natural granite selected from a quarry in Sichuan Province was processed into 150 mm × 150 mm × 150 mm square specimens in the laboratory, and then, the specimens were split using the Brazilian splitting test method to obtain artificial tensional joint specimens. Finally, five groups of fracture surfaces (F1, F2, F3, F4, and F5) with different roughness were prepared.

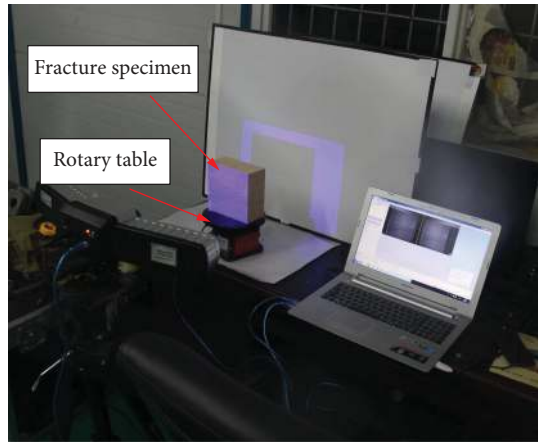

Figure 1: Stereo topometric scanning system.

3.2. Measurement Procedure. A portable 3D optical three-dimensional scanning system was used to measure the three-dimensional morphology of the fracture surface (Figure 1). The system broadly comprises a scanning control unit, scanning lens, turn table, and tripod. The scanning lens is placed on the tripod, which can rotate freely and adjust its position conveniently. The other components are connected via USB. The system acquires a visible grating image projected onto the surface of the object then accurately determines the spatial coordinates (X, Y, Z) of each point using the phase and triangulation methods according to the shape of fringe curvature change, forming a three-dimensional point cloud data. This approach has the benefits of being fast, high precision (measuring accuracy 25 μm), and allowing noncontact measurement.

In the actual measurement process, features of the measurement environment (light, dust, etc.) and the measurement methods will have an impact on the accuracy of the three-dimensional topographic data. Therefore, after acquiring the three-dimensional data for a fracture surface, the point cloud data were processed by using the self-contained software CloudForm to reduce noise, remove irrelevant points, filter data ripples, and patch. Additionally, the original point cloud of the fracture surface is composed of hundreds of thousands of discrete points with an average spacing of 0.025 mm, which amount to a huge amount of disordered data. Data analysis was facilitated by compiling the program with MATLAB software to delete and reorder the measured points. The newly obtained fracture surface has a total of 22801 points at an average spacing of 1 mm. The measured topographic parameters of the fracture surfaces shown in Figure 2 are listed in Table 1.

4. Calculation of Fractal Dimension

There are many methods for calculating the fractal dimension of a rough fracture surface. Clarke [30] first proposed

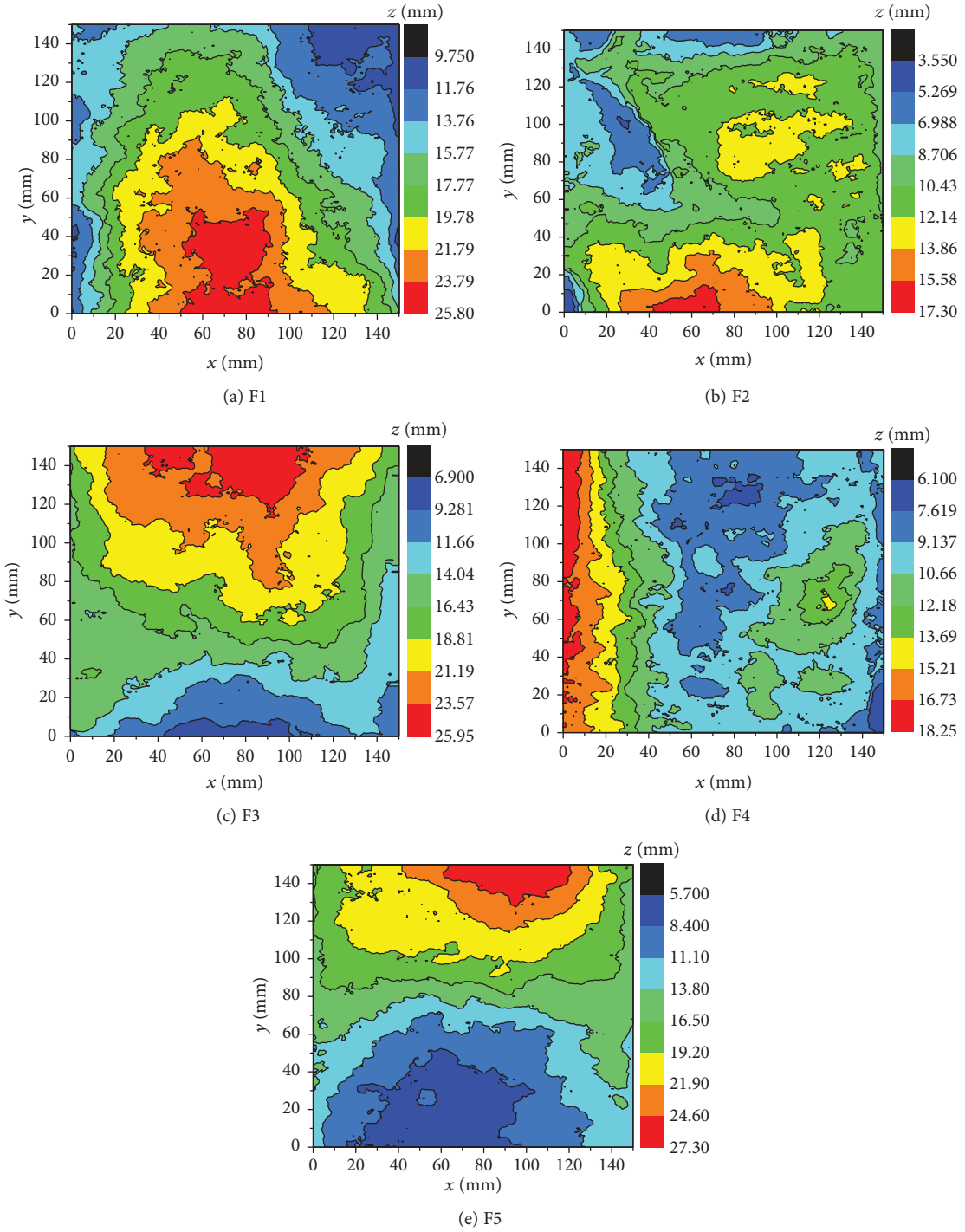

Figure 2: Surfaces topographies of fractures (lower surfaces).

Table 1: Geometrical details of fractures.

Specimen	Length L (mm)	Width w (mm)	Peak asperity height ξ (mm)	Variance R_{rms} (mm^2)	Average R_m (mm)	JRC
F1	149.9	150.1	3.74	2.06	1.58	11.3
F2	150.1	150.0	3.65	2.07	1.55	11.0
F3	150.1	150.1	3.97	4.14	3.52	12.8
F4	150.2	149.9	4.89	5.16	4.39	16.9
F5	150.1	149.9	3.27	3.87	3.29	13.9

the triangular prism surface area method, which takes the spatial surface area as the variable and a square grid as the measure scale. Later, Xie and Wang [23] proposed a projection coverage method. These two methods can be categorized as driver methods. The dimension calculated by these two methods is a similar fractal dimension, not a geometric fractal dimension. Zhou et al. [19] proposed box-counting methods for calculating the fractal dimension of a three-dimensional surface, including a cube coverage method and an improved cube coverage method. The above computational theories are based on statistical self-similarity. However, Brown [31] and Kulatilake et al. [32, 33] argue that rough rock fracture surfaces conform to the characteristics of a self-affine model.

Kulatilake et al. [32] put forward a variogram method as a self-affine model to determine the fractal dimension. This takes the variogram function $2\gamma(x, h)$ of the profile as a variable and the interval distance h as the measure scale.

The detailed method is as follows:

Step 1. Generation of two-dimensional contour data in different directions. Firstly, the fracture surface data are meshed into 1 mm × 1 mm grids. 2D profiles are divided from the fracture surface data in accordance with the directions $\theta = 15 \times k\,(k = 1, 2, \cdots, 11)$. The height data $Z(x, y)$ of a directional line is then calculated. The height data Z_Q of the coordinate $Q(x, y)$ is found on the 15-degree directional line P. The height of the coordinate radius within a 1 mm range is calculated according to equation (17). The profile data are then obtained cyclically. The next set of profile data with a distance of 10 mm is obtained by the same method. Finally, the profile data in each direction are obtained by repeated cyclic calculation.

$$Z(x, y) = \frac{\sum_{i=1}^{n} Z_i / r_i}{\sum_{i=1}^{n} 1 / r_i}, \tag{17}$$

where Z_i is the height of the point within a radius of 1 mm from point Q and r_i is the distance from point i to point Q.

Step 2. Calculation of the fractal dimension of all of the directional lines. The variogram function is defined as

$$2\gamma(h) = \frac{1}{N} \sum_{i=1}^{N} [Z_{i+1} - Z_i]^2, \tag{18}$$

where $\gamma(h)\,[\mathrm{L}^2]$ is the semivariogram, $Z_i\,[\mathrm{L}]$ and $Z_{i+1}\,[\mathrm{L}]$ are the heights of the 2D profile from the baseline, and N is the number of pairs of Z at a lag distance (h) between them. $\gamma(h)$ can be simplified as a power-law function in the self-affine profile as $h \to 0$:

$$2\gamma(h) = K_v h^{2H}, \tag{19}$$

where K_v is a proportionality constant and H is the Hurst exponent, which is related to the fractal dimension by $D_v = 2 - H$. However, equation (18) and equation (19) cannot be used to calculate D_v directly. D_v should be written in the logarithmic form

$$\log(2\gamma(h)) = 2(2 - D_v) \log h + \log K_v, \tag{20}$$

so that D_v can be obtained by linear regression analysis. At least seven variance functions at different intervals h are calculated for each profile line, and fractal dimension D is obtained by fitting equation (20). The fractal dimension D of all of the profiles in one direction is averaged, and the fractal dimension D in that direction is obtained.

To make the anisotropic characteristics of fracture surface roughness more intuitive, Table 2 presents rose diagrams of the fractal dimensions of five different fracture surfaces (F1–F5). The fractal dimension is randomly distributed in all directions, and the fracture surfaces are characterized by an irregular anisotropic roughness structure. The fractal dimension of the fracture surface of F4 is larger than that of the others and is the highest, 1.60, in the 90° direction. Therefore, F4 has the greatest roughness of the fracture surfaces.

It is noted that the fractal dimension D does not take the difference between forward and backward on the 2D profile into consideration. For example, the fractal dimension of the 0° profile is the same as that of 180°. Hence, equation (20) is correct when assuming there is the same nonlinear flow in the θ and $\theta + 180°$ directions.

5. Nonlinear Flow Behavior of Rough-Walled Rock Fractures

5.1. Seepage Tests of Rough-Walled Rock Fractures. The five groups of rock fracture surfaces (F1–F5) mentioned in the previous section were prepared for flow testing with a self-designed device. A detailed description of the device is given in Xiong et al. [7]. Two flow directions (0° and 90°) were tested for each group of fractures, as shown in Figure 3. The pressure difference P under different flow rates Q was recorded during the test process; flow rates were in the range 0–100 ml/s during the tests.

5.2. Nonlinear Flow Behavior. Figures 4 and 5 show the relationship between the flow rate Q and the pressure gradient ∇P of each fracture in the 0° and 90° directions. When the flow rate is small ($Q < 10$ ml/s), the pressure gradient increases linearly with the flow rate. When the flow rate increases, the pressure gradient increases nonlinearly, showing an increase in the inertia effect. In order to describe this relationship, the Forchheimer formula was used to fit the test data for the 0° and 90° directions. The fitting results are shown in Table 3. These results indicate that Forchheimer's law (equation (1)) is able to quantitatively describe the nonlinear flow behavior, which is consistent with Zimmerman et al. [17].

In order to analyze the anisotropic characteristics of flow in a rock fracture, a new parameter describing anisotropy is

Table 2: The fractal dimensions at different directions.

Directions (°)	F_1	F_2	F_3	F_4	F_5
0	1.422	1.497	1.421	1.418	1.475
30	1.398	1.486	1.391	1.426	1.426
60	1.431	1.477	1.417	1.486	1.435
90	1.542	1.503	1.434	1.600	1.436
120	1.478	1.466	1.471	1.489	1.389
150	1.425	1.459	1.370	1.424	1.407
180	1.422	1.497	1.421	1.418	1.475
210	1.398	1.486	1.391	1.426	1.426
240	1.431	1.477	1.417	1.486	1.435
270	1.542	1.503	1.434	1.600	1.436
300	1.478	1.466	1.471	1.489	1.389
330	1.425	1.459	1.370	1.424	1.407

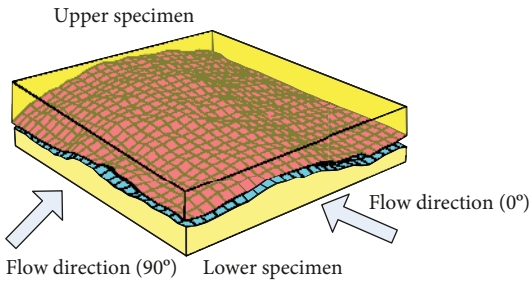

Figure 3: Different directions of flow (0° and 90°) in a rock fracture.

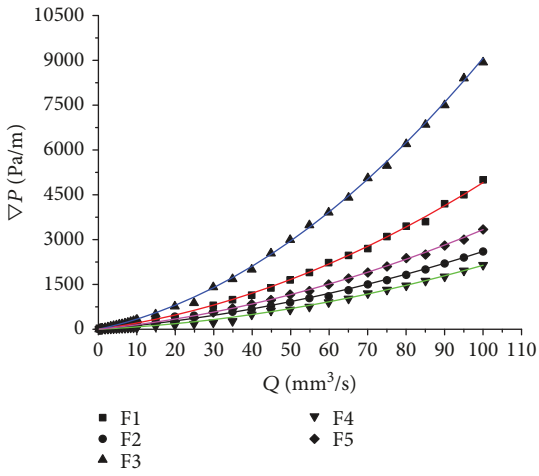

Figure 4: Relationship between pressure gradient and flowrate in the 0° direction.

proposed: the ratio of the difference between the 90° and 0° pressure gradients and the 90° pressure gradient.

$$\text{anisotropy} = \frac{\nabla P_{90^\circ} - \nabla P_{0^\circ}}{\nabla P_{90^\circ}}, \tag{21}$$

where ∇P_{90° is the pressure gradient in the 90° direction and ∇P_{0° is the pressure gradient in the 0° direction. Figure 6 shows the variation of anisotropy with flow rate. The anisotropy values differ between the different groups, which indicate that the anisotropy of fracture flow exists and is related to the fracture morphology and aperture distribution.

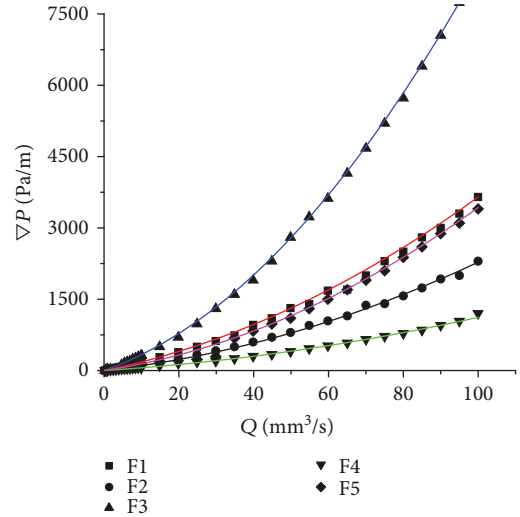

Figure 5: Relationship between pressure gradient and flowrate in the 90° direction.

Normalized transmissivity (T_a/T_0) is determined by Zimmerman et al. [17] in the following form:

$$\frac{T_a}{T_0} = \frac{1}{1 + \beta\,\mathrm{Re}}, \tag{22}$$

where T_a is the apparent transmissivity and T_0 is a special apparent transmissivity in Darcy's flow state and is typically called intrinsic transmissivity. According to experimental data, the values of β are listed in Table 2. The relationship of b_D and β is plotted in Figure 7. It can be seen from the figure that as b_D increases, β linearly increases. And β is about 12 times than b_D, which is consistent with Zimmerman et al. [17].

5.3. Verification of the Nonlinear Flow Model Based on Fractal Theory. In order to solve the undetermined constants a and b, fracture morphology data were first obtained for F1, F2, and F3, and the fractal dimension was then calculated according to the method detailed in Section 4. Then, the seepage test results were fitted according to the Levenberg-Marquardt method, and the parameters a and b were found to be 0.246 and -0.964, respectively.

In order to verify the model, the nonlinear fractal model is compared with the seepage test data and Chen's two-parameter model [6].

For fractures F4 and F5, pressure gradients were calculated according to the proposed model and the Chen model, respectively, and the results were compared with the experimental values, as shown in Figure 8. It can be seen that the results calculated with the nonlinear fractal model are close to the measured values, and the relative errors are mostly within 20%. This shows that the nonlinear fractal model gives a better description of nonlinear seepage in fractured media

Table 3: Fractal dimension and fitted parameters of Forchheimer's law.

Specimen		$A \times 10^6$ (Kg·s^{-1}·m^{-5})	$B \times 10^{10}$ (Kg·m^{-8})	e_h (mm)	Re$_c$	D	b_D	β
F1	0°	17.62	31.47	1.656	33.90	1.4221	0.00322	0.0027
	90°	15.97	20.50	1.711	56.18	1.542	0.0232	0.002
F2	0°	11.04	15.01	1.935	43.53	1.497	0.0245	0.0021
	90°	8.78	14.21	2.089	42.97	1.503	0.0292	0.0023
F3	0°	27.56	63.18	1.427	35.88	1.421	0.0414	0.0033
	90°	27.47	56.93	1.428	38.03	1.434	0.0374	0.003
F4	0°	6.30	15.10	2.333	28.99	1.418	0.0433	0.0035
	90°	5.09	6.09	2.504	57.82	1.600	0.0216	0.0018
F5	0°	13.07	20.08	1.829	40.84	1.475	0.0277	0.0022
	90°	18.96	2.24	1.890	34.12	1.436	0.0034	0.00026

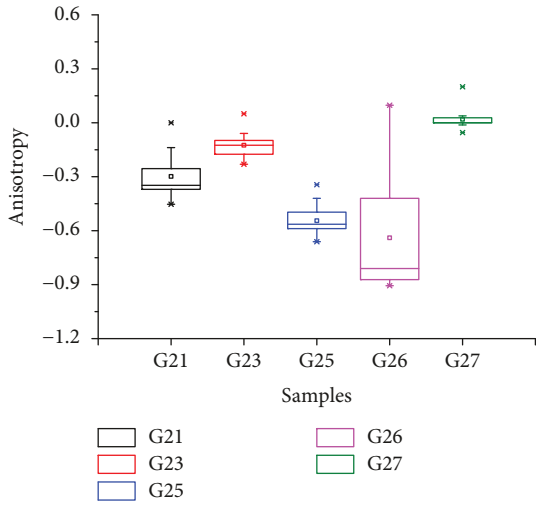

Figure 6: Pressure anisotropy of fracture samples F1–F5.

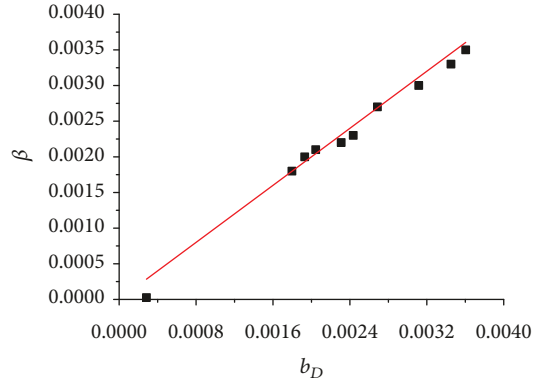

Figure 7: The relationships of b_D and β of fracture samples F1–F5.

than does Chen's model. The error is larger in Chen's model because absolute roughness is not sufficient to quantify the effect of surface topography on fracture flow.

6. Discussion

Forchheimer's law has been widely applied for nonlinear seepage flow in fractured media, but the mechanism of the transition from linear flow to nonlinear flow needs to be further discussed.

Zimmerman et al. (2014) considered the linear to nonlinear transition process in fracture fluid flow, distinguishing the two flow regimes by the nonlinear Darcy effect factor α with a value of 0.1:

$$\alpha = \frac{BQ^2}{AQ + BQ^2}. \tag{23}$$

Therefore, many scholars have used the critical Reynolds number to describe the transition mechanism. For fractured media, the Reynolds number can be expressed as follows:

$$\mathrm{Re} = \frac{\rho Q}{\mu w}. \tag{24}$$

By substituting equation (16) and equation (23) into equation (24), a new critical Reynolds number can be obtained:

$$\mathrm{Re}_c = 5.42\left(\frac{e_h}{L_c}\right)^{-0.964(D_l-1)}. \tag{25}$$

Equation (25) shows that the critical Reynolds number is closely related to hydraulic aperture, the fractal dimension of the fracture surface, and the flow direction. The smaller the hydraulic aperture and the rougher the fracture surface, the smaller the critical Reynolds number. The critical Reynolds numbers calculated by this method are shown in Table 2. Its value ranges between 30 and 60, much smaller than the 2300 value considered by Wang et al. (2015). The nonuniform distributions of the fracture aperture and the rough surface result in eddy currents and reflux flow, which make the flow tortuous and increase the inertial resistance. This leads to nonlinear flow at a low Reynolds number.

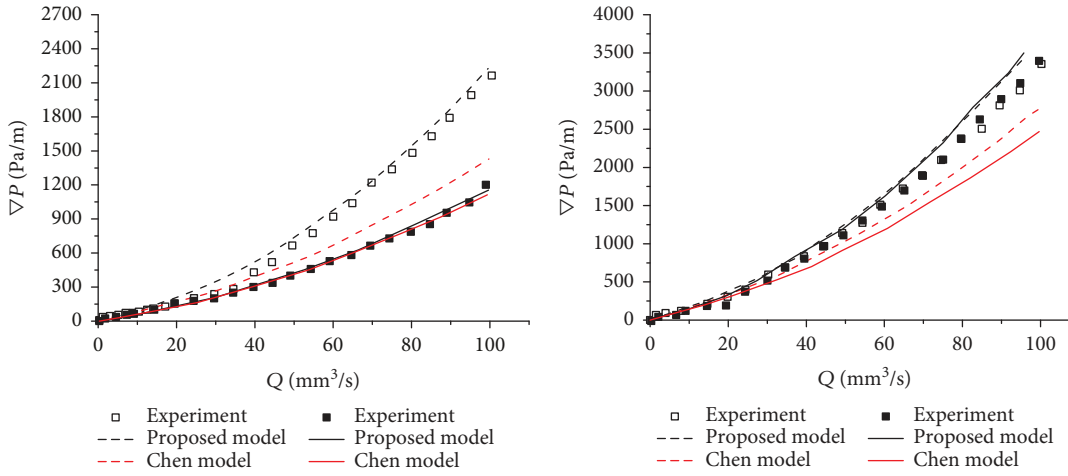

(a) F4 (b) F5

FIGURE 8: Comparison of results from equation (21), equation (22), and experimental measurements (open point is flow test along the 0° direction and solid point is flow test along the 90° direction; dashed line and solid line are proposed and the Chen model in 0° and 90° directions, respectively).

7. Conclusions

This paper discusses the effect of roughness on nonlinear flow in a rock fracture based on previous research and analysis of physical laboratory experiments. The main conclusions are as follows:

(1) A new nonlinear seepage model for rough fractures, equation (16), is proposed according to flow tortuosity in the fracture and the fractal characteristics of the fracture

(2) The 3D optical three-dimensional scanning system was used to acquire point cloud data from fracture surfaces. The self-affine fractal dimension calculation method proposed by Kulatilake et al. [32] was used to analyze the anisotropic characteristics of the roughness of the fracture surface

(3) Five different kinds of rough fractures were tested in seepage experiments in the 0° and 90° directions. The results show that fracture flow conforms to Forchheimer's law and has clear isotropic characteristics. The new model generates results that are closer to those from the experiment than does Chen's two-parameter model

(4) According to the new model, a new expression of the critical Reynolds number (equation (25)) for distinguishing Darcy flow from Forchheimer flow is proposed. It shows that the critical Reynolds number is closely related to hydraulic aperture, the roughness of the fracture surface, and the flow direction

Data Availability

The data are all available and have been explained in this article; readers can access the data supporting the conclusions of the study.

Conflicts of Interest

The authors declare that they have no conflicts of interest

Authors' Contributions

Chun Zhu and Yun Lin contributed equally to this work.

Acknowledgments

This work was supported by the Key Research and Development Project of Zhejiang Province (Grant No. 2019C03104) and the Special Funds of Fundamental Research Funds for Central Universities (2015QB02). The first author is grateful to the Chinese Scholarship Council and the University of Adelaide for providing an opportunity to conduct this research as a joint Ph.D. student.

References

[1] W. P. Huang, C. Li, L. W. Zhang, Q. Yuan, Y. S. Zheng, and Y. Liu, "In situ identification of water-permeable fractured zone in overlying composite strata," *International Journal of Rock Mechanics and Mining Sciences*, vol. 105, pp. 85–97, 2018.

[2] Y. Li, S. Zhang, and X. Zhang, "Classification and fractal characteristics of coal rock fragments under uniaxial cyclic loading conditions," *Arabian Journal of Geosciences*, vol. 11, no. 9, p. 201, 2018.

[3] X. Wang and L. Tian, "Mechanical and crack evolution characteristics of coal–rock under different fracture-hole conditions: a numerical study based on particle flow code," *Environmental Earth Sciences*, vol. 77, no. 8, p. 297, 2018.

[4] Z. Wu, H. Sun, and L. N. Y. Wong, "A cohesive element-based numerical manifold method for hydraulic fracturing modelling with voronoi grains," *Rock Mechanics and Rock Engineering*, pp. 1–25, 2019.

[5] S. C. Zhang, Y. Y. Li, B. T. Shen, X. Sun, and L. Gao, "Effective evaluation of pressure relief drilling for reducing rock bursts

and its application in underground coal mines," *International Journal of Rock Mechanics and Mining Sciences*, vol. 114, pp. 7–16, 2019.

[6] Y. F. Chen, J. Q. Zhou, S. H. Hu, R. Hu, and C. B. Zhou, "Evaluation of Forchheimer equation coefficients for non-Darcy flow in deformable rough-walled fractures," *Journal of Hydrology*, vol. 529, pp. 993–1006, 2015.

[7] F. Xiong, Q. Jiang, Z. Ye, and X. Zhang, "Nonlinear flow behavior through rough-walled rock fractures: the effect of contact area," *Computers and Geotechnics*, vol. 102, pp. 179–195, 2018.

[8] F. Xiong, Q. Jiang, C. Xu, X. Zhang, and Q. Zhang, "Influences of connectivity and conductivity on nonlinear flow behaviours through three-dimension discrete fracture networks," *Computers and Geotechnics*, vol. 107, pp. 128–141, 2019.

[9] C. Yao, C. He, J. Yang, Q. Jiang, J. Huang, and C. Zhou, "A novel numerical model for fluid flow in 3D fractured porous media based on an equivalent matrix-fracture network," *Geofluids*, vol. 2019, Article ID 9736729, 13 pages, 2019.

[10] Z. Ye, Q. Jiang, C. Yao et al., "The parabolic variational inequalities for variably saturated water flow in heterogeneous fracture networks," *Geofluids*, vol. 2018, Article ID 9062569, 16 pages, 2018.

[11] R. W. Zimmerman and G. S. Bodvarsson, "Hydraulic conductivity of rock fractures," *Transport in Porous Media*, vol. 23, no. 1, pp. 1–30, 1996.

[12] S. Gentier, D. Hopkins, and J. Riss, "Role of fracture geometry in the evolution of flow paths under stress," in *Dynamics of Fluids in the Fractured Rock*, pp. 169–184, American Geophysical Union, 2000.

[13] T. Ishibashi, N. Watanabe, N. Hirano, A. Okamoto, and N. Tsuchiya, "Beyond-laboratory-scale prediction for channeling flows through subsurface rock fractures with heterogeneous aperture distributions revealed by laboratory evaluation," *Journal of Geophysical Research: Solid earth*, vol. 120, no. 1, pp. 106–124, 2014.

[14] Q. Jiang and C. Zhou, "A rigorous solution for the stability of polyhedral rock blocks," *Computers and Geotechnics*, vol. 90, pp. 190–201, 2017.

[15] T. Zhigang, Z. Chun, W. Yong, W. Jiamin, H. Manchao, and Z. Bo, "Research on stability of an open-pit mine dump with fiber optic monitoring," *Geofluids*, vol. 2018, Article ID 9631706, 20 pages, 2018.

[16] P. A. Witherspoon, "Investigation at Berkeley on fracture flow in rocks: from the parallel plate model to chaotic systems," in *Dynamics of Fluid in Fractured Rocks*, B. Faybishenko, S. Benson, and P. Witherspoon, Eds., pp. 1–58, American Geophysical Union, Washington, DC, USA, 2000.

[17] R. W. Zimmerman, A. al-Yaarubi, C. C. Pain, and C. A. Grattoni, "Nonlinear regimes of fluid flow in rock fractures," *International Journal of Rock Mechanics and Mining Sciences*, vol. 41, no. 3, pp. 163–169, 2004.

[18] Z. Zhang and J. Nemcik, "Fluid flow regimes and nonlinear flow characteristics in deformable rock fractures," *Journal of Hydrology*, vol. 477, no. 1, pp. 139–151, 2013.

[19] J.-Q. Zhou, S.-H. Hu, S. Fang, Y.-F. Chen, and C.-B. Zhou, "Nonlinear flow behavior at low Reynolds numbers through rough-walled fractures subjected to normal compressive loading," *International Journal of Rock Mechanics and Mining Sciences*, vol. 80, pp. 202–218, 2015.

[20] Y. W. Tsang, "The effect of tortuosity on fluid flow through a single fracture," *Water Resources Research*, vol. 20, no. 9, pp. 1209–1215, 1984.

[21] W. Xiao, C. Xia, W. Wang, and Y. Bian, "Study on calculation of fluid flow through a single rough joint by considering flow tortuosity effect," *Chinese Journal of Rock Mechanics and Engineering*, vol. 30, no. 9, pp. 2416–2425, 2011.

[22] N. Watanabe, N. Hirano, and N. Tsuchiya, "Diversity of channeling flow in heterogeneous aperture distribution inferred from integrated experimental-numerical analysis on flow through shear fracture in granite," *Journal of Geophysical Research*, vol. 114, pp. 115–123, 2009.

[23] H. Xie and J. Wang, "Direct fractal measurement of fracture surfaces," *International Journal of Solids and Structures*, vol. 36, no. 20, pp. 3073–3084, 1999.

[24] S. Murata and T. Saito, "Estimation of tortuosity of fluid flow through a single fracture," *Journal of Canadian Petroleum Technology*, vol. 42, no. 12, pp. 39–45, 2003.

[25] G. Wang, N. Huang, Y. Jiang, B. Li, W. Xuezhen, and X. Zhang, "Seepage calculation model for rough joint surface considering fracture characteristics," *Chinese Journal of Rock Mechanics and Engineering*, vol. 33, pp. 3397–3405, 2014.

[26] Y. Ju, Q. G. Zhang, Y. M. Yang, H. P. Xie, F. Gao, and H. J. Wang, "An experimental investigation on the mechanism of fluid flow through single rough fracture of rock," *Science China Technological Sciences*, vol. 56, no. 8, pp. 2070–2080, 2013.

[27] K. Develi and T. Babadagli, "Experimental and visual analysis of single-phase flow through rough fracture replicas," *International Journal of Rock Mechanics and Mining Sciences*, vol. 73, pp. 139–155, 2015.

[28] T. W. Schrauf and D. D. Evans, "Laboratory studies of gas flow through a single natural fracture," *Water Resources Research*, vol. 22, no. 7, pp. 1038–1050, 1986.

[29] Y. Jin, J. L. Zheng, J. B. Dong, C. H. Huang, X. Li, and Y. Wu, "Fractal seepage law characterizing fluid flow through a single rough cleat composed of self-affine surfaces," *Chinese Science Bulletin*, vol. 60, no. 21, pp. 2036–2047, 2015.

[30] K. C. Clarke, "Computation of the fractal dimension of topographic surfaces using the triangular prism surface area method," *Computers and Geosciences*, vol. 12, no. 5, pp. 713–722, 1986.

[31] S. R. Brown, "Fluid flow through rock joints: the effect of surface roughness," *Journal of Geophysical Research: Solid Earth*, vol. 92, no. B2, pp. 1337–1347, 1987.

[32] P. H. S. W. Kulatilake, P. Balasingam, J. Park, and R. Morgan, "Natural rock joint roughness quantification through fractal techniques," *Geotechnical and Geological Engineering*, vol. 24, no. 5, pp. 1181–1202, 2006.

[33] P. H. S. W. Kulatilake, J. Park, P. Balasingam, and R. Morgan, "Quantification of aperture and relations between aperture, normal stress and fluid flow for natural single rock fractures," *Geotechnical and Geological Engineering*, vol. 26, no. 3, pp. 269–281, 2008.